metals

MDPI

Article

Effects of Multi-Phase Reinforcements on Microstructures, Mechanical and Tribological Properties of Cu/Ti_3SiC_2/C/BN/GNPs Nanocomposites Sintered by Vacuum Hot-Pressing and Hot Isostatic Pressing

Zhenyi Shao [1,2], Yue Sun [2], Wanxia Liu [2], Xueqiao Zhang [2] and Xiaosong Jiang [2,*]

[1] School of Materials Engineering, Chengdu Technological University, Chengdu 611730, China; zysao_10227@163.com

[2] School of Materials Science and Engineering, Southwest Jiaotong University, Chengdu 610031, China; 18380175785@163.com (Y.S.); wanxialiu@126.com (W.L.); 18482189480@163.com (X.Z.)

* Correspondence: xsjiang@home.swjtu.edu.cn; Tel.: +86-28-876-007-79

Academic Editor: Hugo F. Lopez

Received: 18 October 2016; Accepted: 14 December 2016; Published: 21 December 2016

Abstract: Cu/Ti_3SiC_2/C/BN/GNPs nanocomposites were prepared by vacuum hot-pressing (HP) sintering and hot isostatic pressing (HIP) sintering methods. Microstructures, mechanical and tribological properties of Cu/Ti_3SiC_2/C/BN/GNPs nanocomposites were investigated. Microstructures were examined by optical microscopy (OM), X-ray diffraction (XRD) and scanning electron microscope (SEM). Mechanical properties were determined by the relative density, micro-Vickers hardness, as well as tensile strength, compressive strength and shear strength. Tribological behavior of the Cu/Ti_3SiC_2/C/BN/GNPs composite against the GCr15 steel ring was evaluated using an M-2000 wear tester with high tangential sliding velocity. Results demonstrated that BN and graphene nano-platelets (GNPs) have an impact on the microstructures and mechanical properties of Cu/Ti_3SiC_2/C/BN/GNPs nanocomposites. Based on microstructures, and mechanical and tribological properties of Cu/Ti_3SiC_2/C/BN/GNP nanocomposites, strengthening, fracture and wear mechanisms for synergistic enhancement by multi-phase reinforcements were analyzed.

Keywords: Cu/Ti_3SiC_2/C/BN/GNPs nanocomposites; hot isostatic pressing; microstructure; mechanical properties; wear

1. Background

Copper matrix self-lubricating composites are widely used in many industrial applications, such as friction materials, bearings, bushes, brake pads/discs, electrical sliding contacts and fusion reactors, due to their excellent anti-friction, wear properties, good thermal, electrical conductivities, superior strength and ease of production [1–6]. As many reports have revealed, copper-graphite is one of the most often-used solid self-lubricating materials for graphite's lamellar structure [6], and copper-graphite composites have improved wear resistance, lower wear loss and friction coefficients than pure copper [7,8]. However, the main inadequacy of using graphite as self-lubricant is the unsatisfactory mechanical properties of the composites [9,10]. Due to the impressive thermal, electrical, mechanical and tribological properties, graphene is a promising reinforcement for copper matrix, and an increasing number of researches have examined Cu/graphene composites aiming to improve their mechanical and tribological properties [4,9,11]. The results reveal that the presence of graphene in matrix can not only improve the mechanical properties but also decrease both the friction coefficient and the wear rate of composites [12]. Nevertheless, the agglomeration of graphene nano-platelets (GNPs) and interfacial interactions significantly affect the strengthening efficiency of

GNPs; a number of works have been carried out to solve these problems [13]. Though hexagonal boron nitride (h-BN) has a similar structure to graphite, it has some particular properties, such as high thermal conductivity, good chemical inertness, and high thermal stability [14]. Several studies have demonstrated that h-BN has a significant effect on the reduction of friction efficient and wear loss of Cu/BN composites because BN forms a lubricant film on the friction surfaces [15–17]. In addition, Ti_3SiC_2 has unique properties combining metal and ceramics attributes, especially the high thermal conductivity and the matching thermal expansion coefficients of Ti_3SiC_2 and Cu, making Ti_3SiC_2 a promising reinforcement for copper [18,19]. The previous results have demonstrate that Ti_3SiC_2 has a beneficial effect on mechanical properties as well as the tribological performance of copper matrix composites [19,20].

A number of studies have been carried out on a single or dual-phase reinforced metal matrix composite, but only limited researches are available on the properties of multiphase reinforced Cu matrix nanocomposites. Sundararajan et al. [6] have reported that graphite and ceramic (SiC) reinforced Cu matrix composite shows improved mechanical properties, a better wear resistance and friction coefficient compared to copper without any reinforcements, which suggests the great potential of multi-phase reinforced Cu matrix composites.

In this paper, the components of h-BN and graphite are proposed to improve the self-lubricating property of composites, meanwhile, GNPs and Ti_3SiC_2 are proposed to improve the mechanical properties and tribological properties of the composites without conductivity gradation. Vacuum hot-pressing sintering combined with hot isostatic pressing sintering method were presented to prepare Cu/Ti_3SiC_2/C/BN/GNPs nanocomposites. To explore the synergistic effects of multi-phase reinforcements on the nanocomposites, microstructures, and mechanical and tribological properties of the Cu/Ti_3SiC_2/C/BN/GNPs nanocomposites were systematically characterized. Furthermore, strengthening, fracture and wear mechanisms of the nanocomposites were analyzed.

2. Methods

2.1. Materials and Procedure

The design of Cu/Ti_3SiC_2/C/BN/GNPs nanocomposite materials is based on the concept of multi-phase composites. GNPs, h-BN, graphite powders, Ti_3SiC_2 powders and electrolytic copper powders were used as raw materials, which are listed in Table 1. The weight percentage of Cu, Ti_3SiC_2, C, BN, and GNPs were 85.5%, 10%, 3%, 1% and 0.5%, respectively. In order to improve the dispersity of GNPs, the non-covalent surface modification and covalent surface modification of GNPs by 0.02 μg/mL rutin aqueous were conducted. The composites were prepared by powder metallurgy of vacuum hot-pressing sintering combined with hot isostatic pressing sintering. Firstly, the GNPs and copper powders were mixed for 20 min, then, according to their density, graphite, BN and Ti_3SiC_2 were added in sequence and mixed for 1 h. Both of the mixing procedures were conducted on a planetary ball mill with Polyurethane mill jars and agate balls, and the tert-Butanol acted as the milling medium. The mixture was further freeze-dried into composite powder, which was subsequently hot pressed in a vacuum-sintering furnace under 950 °C with the pressure of 20 MPa for 2 h before being cooled inside the furnace to room temperature; secondly, the sample was compacted by hot isostatic pressing sintering, through being heated from room temperature to 650 °C at a heating rate of 10 °C/min under the pressure of 0.6 MPa applied on the sample, then the final sintering was carried out at 900 °C with the pressure of 100 MPa for 2 h in an Ar atmosphere before being rapidly cooled (a cooling rate of 20 °C/min) to room temperature.

Table 1. Raw material powder properties.

Materials	Density (g/cm^3)	Granularity (Mesh)	Purity (wt. %)	Remarks
GNPs	2.25		>99.8	Less than 10 layers
h-BN	2.1	μm	≥99.99	
Graphite	2.2	200		
Ti_3SiC_2	4.53	300		
Copper	8.89	250	≥99.99	Electrolytic copper powder

Relative density of Cu/Ti_3SiC_2/C/BN/GNPs nanocomposites was evaluated by the Archimedes method. To explore the interactions among different phases in raw materials during the sintering process, X-ray diffraction (XRD) analysis of the nanocomposite were carried out using X'PertPro-MPD (PANalytical B.V., Almelo, The Netherlands) with Cu Kα radiation. The morphology and microstructures of the composite powders and nanocomposites were characterized by optical microscopy (OM, AxioCam MRC5, ZEISS, Wetzlar, Germany), and scanning electron microscope (SEM, JEM100CX, JEOL Ltd., Tokyo, Japan) with an energy dispersive X-ray spectrometer (EDS, JEOL Ltd., Tokyo, Japan).

2.2. Mechanical Properties Tests

The hardness value was the average value of eight results measured eight times by micro-Vickers hardness (HXD-100TM/LCD, TaiMing, Shanghai, China) tester. The applied load and holding time were 5000 N and 10 s, respectively. Tensile, compressive and shear tests were conducted on a microcomputer-controlled electronic universal testing machine (WDW-3100 RuiMa, Jinan, China) with a loading speed of 0.5 mm/min. The samples for tensile tests were dog-bone shaped, while the compressive and shear specimens were cylindrical. To investigate the fracture mechanism, the morphology of fractures was observed by SEM examination after each test.

2.3. Wear Tests

Tribological properties were studied by an M-2000 wear tester. Specimens were cuboid with dimensions of 10 mm × 10 mm × 16 mm and the counter part was the GCr15 steel with an outer diameter of 35 mm. Prior to testing, the specimens were ultrasonically cleaned with acetone and alcohol, dried and then measured by an analytical balance before and after each wear test. The applied load and rotational speed were 500 N, 450 N, 400 N, 350 N and 50 rpm, 100 rpm, 150 rpm, and 200 rpm respectively. The total sliding distance was 100 m. During the tests, the friction coefficient was recorded constantly and the average value was calculated for each test within 100 m. In order to investigate the roles that multi-phase reinforcements played during the friction process and the basic wear mechanism involved, worn surfaces and wear debris of the nanocomposites were analyzed by SEM equipped with an energy dispersive X-ray spectrometer (EDS).

3. Results and Discussion

3.1. Characterization of Composite Powders

Scanning electron microscope (SEM) and transmission electron microscope (TEM) images of GNPs provided by Shanghai Chaoqian New Material Technology Company (Shanghai, China) are shown in Figure 1, where Multi-layer folded graphene wrinkles can be observed. In order to characterize the distribution and interactions of GNPs and BN in copper matrix, scanning electron microscopy equipped with an energy dispersive X-ray spectrometer was carried out after each mixing procedure, as shown in Figure 2.

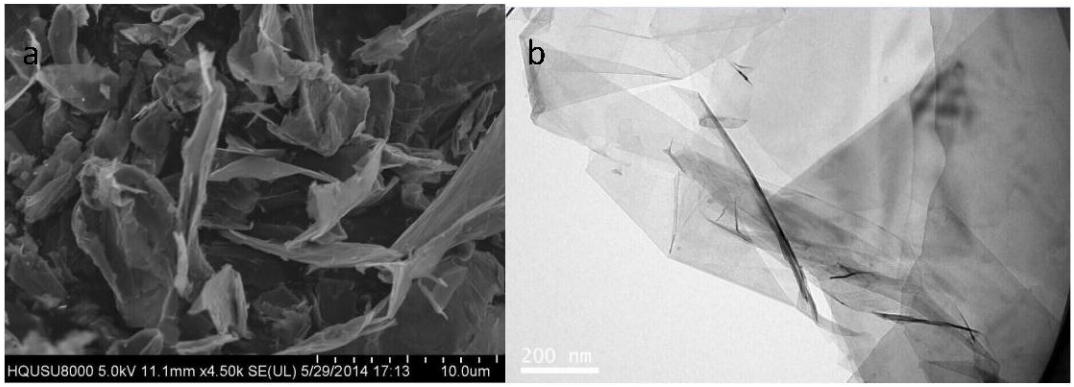

Figure 1. The raw graphene nano-platelets (GNPs) morphology: (**a**) scanning electron microscope (SEM) image; (**b**) transmission electron microscope (TEM) image.

Figure 2a shows the morphology of GNPs/Cu composite powders, where it can be seen that GNPs (arrowed) are homogenously mixed with copper powders and the copper powders became irregular in shape after the ball milling process, while increasing in particle size, which could be attributed to cold-welding of Cu powders. Figure 2b with high magnifications clearly shows that GNPs are adsorbed on the surface or embedded into the Cu matrix, and no visible agglomerations of GNPs were found. The SEM images in Figure 2c,e determined by EDS in Figure 2d,f indicate the existence of BN and GNPs, respectively. In Figure 2e, it is clearly seen that the layered structure with characteristic crumple and fold of GNPs observed by SEM appears in the composite powders, which is similar to that of pure GNPs in Figure 1a and reported previously [13]. This phenomenon implies the morphologies of GNPs keep integrity during the mixing procedures, which may contribute to strengthening nanocomposites, due to the unique texture strengthening mechanism of GNPs [21]. These results illustrate that during ball milling processes Cu powders cold-welded to form larger particles that had rough surfaces [22]. Furthermore, GNPs and BN were uniformly dispersed in Cu powders after ball milling processes, which indicates that the surface modification and ball milling processes executed in the present work is effective to achieve the uniform mixture of the multi-phase reinforcements and Cu powders.

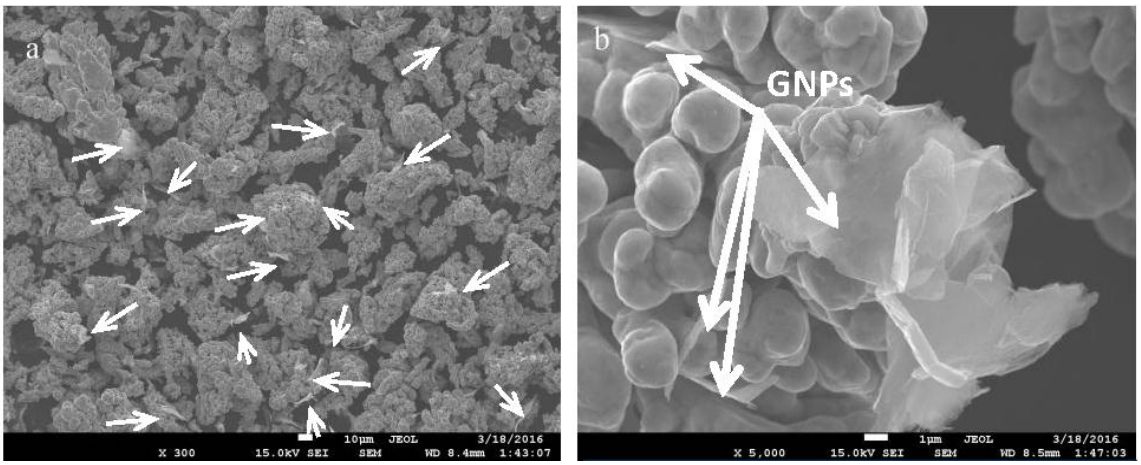

Figure 2. *Cont.*

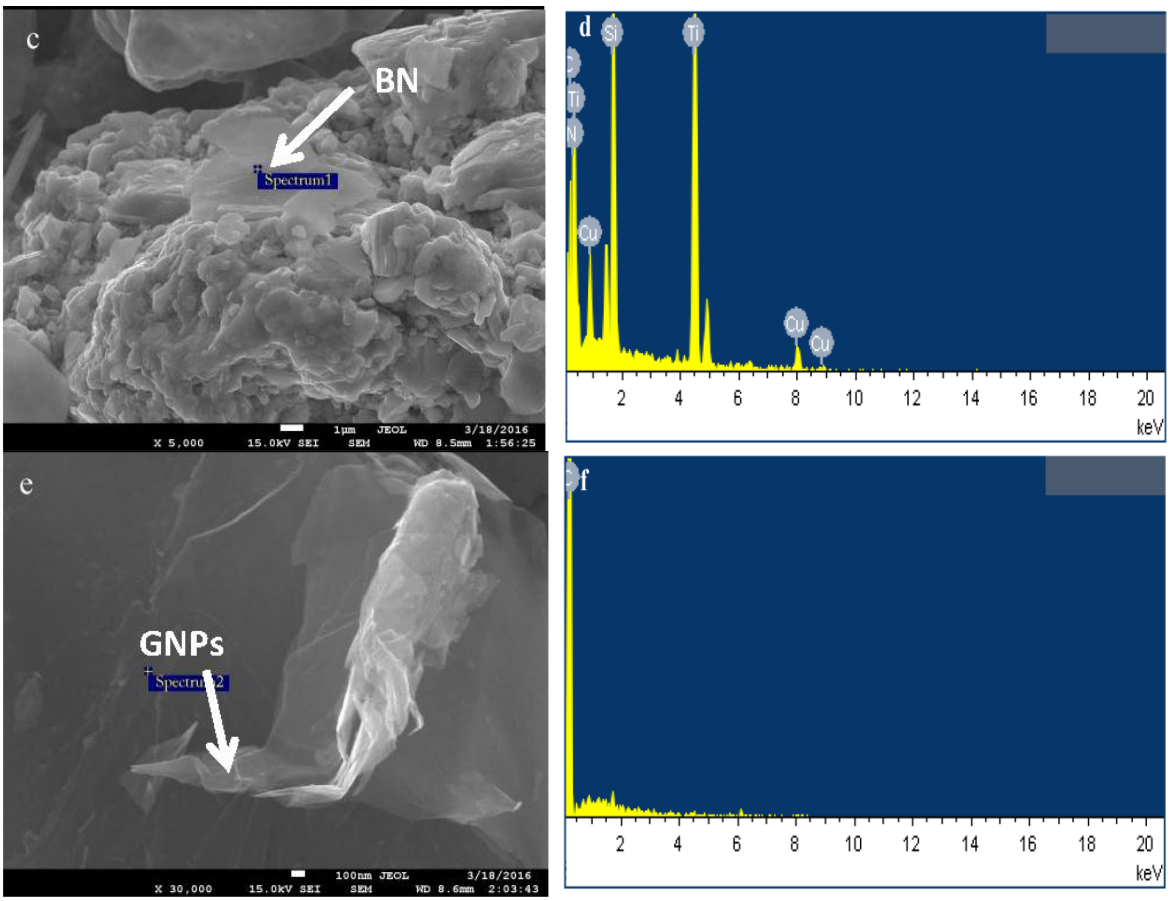

Figure 2. SEM images of the ball-milled powders: (**a**) GNPs/Cu composite powders 300×; (**b**) GNPs/Cu composite powders 5000×; (**c**) Cu/Ti_3SiC_2/C/BN/GNPs composite powders 5000×; (**d**) Energy dispersive X-ray spectrometer (EDS) element analysis of the white flake-like phase marked in (**c**); (**e**) Cu/Ti_3SiC_2/C/BN/GNPs composite powders 30,000×; (**f**) EDS element analysis of the white layered phase marked in (**e**).

3.2. Characterization of Cu/Ti_3SiC_2/C/BN/GNPs Nanocomposites

The sintering process is vital to the relative density of Cu/Ti_3SiC_2/C/BN/GNPs composite. The theoretical density of Cu/Ti_3SiC_2/C/BN/GNPs composite is 7.25 g/cm^3, while the actual density is 7.15 g/cm^3. The relative density of the composite is 98.62%, which belongs to compact material. XRD results of Cu/Ti_3SiC_2/C/BN/GNPs nanocomposites are shown in Figure 3. The diffraction peaks of C and BN were not presented, which may be attributed to the low content of reinforcement phases. Besides, the relative atomic mass of these elements is smaller, resulting in stronger incoherent scatter intensity, therefore, it is difficult to obtain satisfactory diffraction patter of materials containing C, N, B in experiments. The presence of diffraction peaks of Cu, TiC and Cu_9Si manifested that during the sintering process, new phases were produced as described by the following equations:

$$Ti_3SiC_2 = 3TiC_{2/3} + Si \quad (1)$$

$$C + Si = SiC \quad (2)$$

$$SiC + 9Cu = Cu_9Si + C \quad (3)$$

$$Si + 9Cu = Cu_9Si \quad (4)$$

Through thermodynamics calculations, the Gibbs free energy differences of Equation (2) is −63.74 kJ/mol [19] and Equation (4) minus the Equation (3) equals to Equation (2), which indicate that the Gibbs free energy differences of Equation (4) is smaller than that of Equation (3) and the reaction in Equation (3) is difficult to occur than the reaction in Equation (4). The results demonstrate that Ti_3SiC_2 decomposes to TiC and Si when the sintering temperature approached to 1000 °C [23]. Meanwhile, the Si diffused into Cu matrix and form solid solution or intermetallic compounds [24].

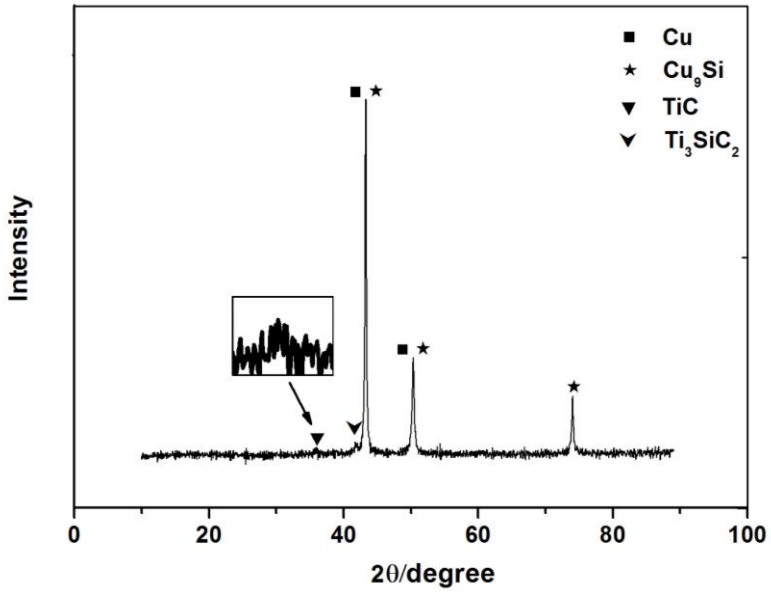

Figure 3. X-ray diffraction (XRD) results of Cu/Ti_3SiC_2/C/BN/GNPs nanocomposites.

Figure 4 presents the metallographic results of composite along parallel direction to that of the compact-pressing. There are many light gray Ti_3SiC_2s that disperse evenly along the grain boundary and it could be observed that the black graphite or GNPs aggregation were scattered within the mass white Cu matrix. Under a 500× microscope, there were no pores visible. The comparison of the metallurgical structure of composite in different directions reveals that the grain size of the copper matrix along parallel direction is slightly finer than that of composite along perpendicular direction as shown in Figure 5.

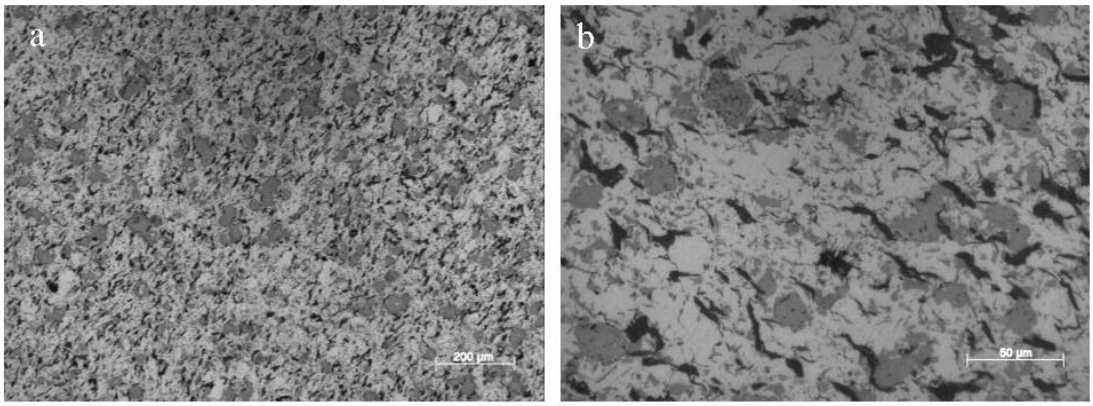

Figure 4. Metallographs of composite along parallel direction to that of the compact-pressing: (**a**) 100×; (**b**) 500×.

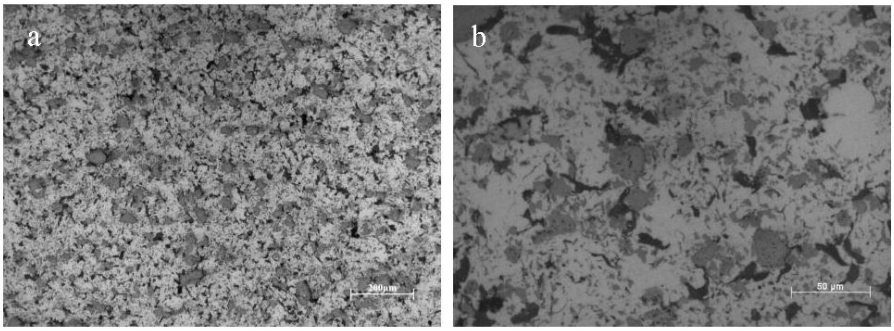

Figure 5. Metallographs of composite along perpendicular direction to that of the compact-pressing: (**a**) 100×; (**b**) 500×.

3.3. Mechanical Properties of $Cu/Ti_3SiC_2/C/BN/GNPs$ Nanocomposites

The average hardness of the nanocomposite is 97.79 HV, which shows an increase in hardness up to 92% compared to annealed pure copper [25]. Increased dislocation density and smaller matrix grain size can result in a higher hardness of the nanocomposites [26]. The stress–strain curves of tensile, compressive and shear tests are plotted in Figure 6. During the tensile tests, the nanocomposite experienced an elastic deformation stage and then brittle failure during uniform plastic deformation without obvious necking. Macro-cracks are straight and perpendicular to the stress direction. The compressive strength of the nanocomposites is 430 MPa. Shear strength reflects the cohesion of the material—namely, the mutual bonding between atoms or molecules in material interiors—and the average shear strength of the nanocomposites is 97 MPa, indicating the interfacial bonding strength between reinforcement phases and the Cu matrix is not adequately strong.

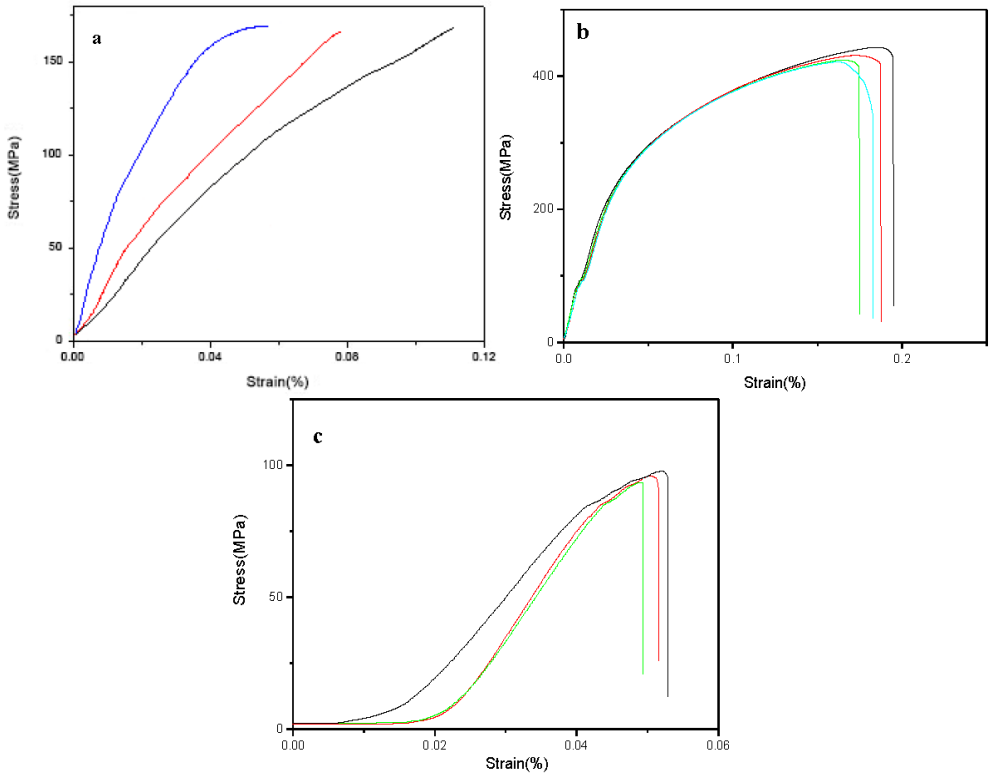

Figure 6. Stress-strain curves of $Cu/Ti_3SiC_2/C/BN/GNPs$ nanocomposites for: (**a**) tensile tests; (**b**) compressive tests; and (**c**) shear tests. (Red, green, and black lines represent three measured results of the specimen for three times).

3.4. Fracture Mechanisms Analysis

The SEM images of tensile fracture surface of Cu/Ti_3SiC_2/C/BN/GNPs are shown in Figure 7. Tensile fracture surfaces of nanocomposites reveal that the fracture is a mixed mode with plastic dimples and decohesion at the interface between reinforcement phases and Cu matrix. As can be observed from Figure 7b, tear ridges exist on the fracture surface, which indicates plastic deformation of the Cu matrix during the tensile tests. Fractographs of shear fracture surface are shown in Figure 8. From Figure 8a, it can be observed that reinforcement phases are wrapped among copper and uniformly distribute in continuous Cu matrix and some pores appear on the fracture surface. During the deformation of nanocomposites, small cracks occur in the peripheral areas of the pores under external load, since the nanocomposites are not completely densified. Figure 8b implies the detachment of GNPs or intergranular fracture occurred in shear tests. Moreover, based on the EDS in Figure 8e, there are cavities of different sizes between GNPs and Cu matrix in Figure 8c. Because of the presence of the voids in the matrix, the nanocomposite is more inclined to initiate crack, then micro-cracks extend along the undesirable interfaces resulting in intergranular fracture of reinforcement phases. Henceforth, it can be concluded that the fracture mechanisms of Cu/Ti_3SiC_2/C/BN/GNPs nanocomposites include micro-porous aggregation fractures and tears of the matrix, interfacial debonding or intergranular fractures of reinforcement phases.

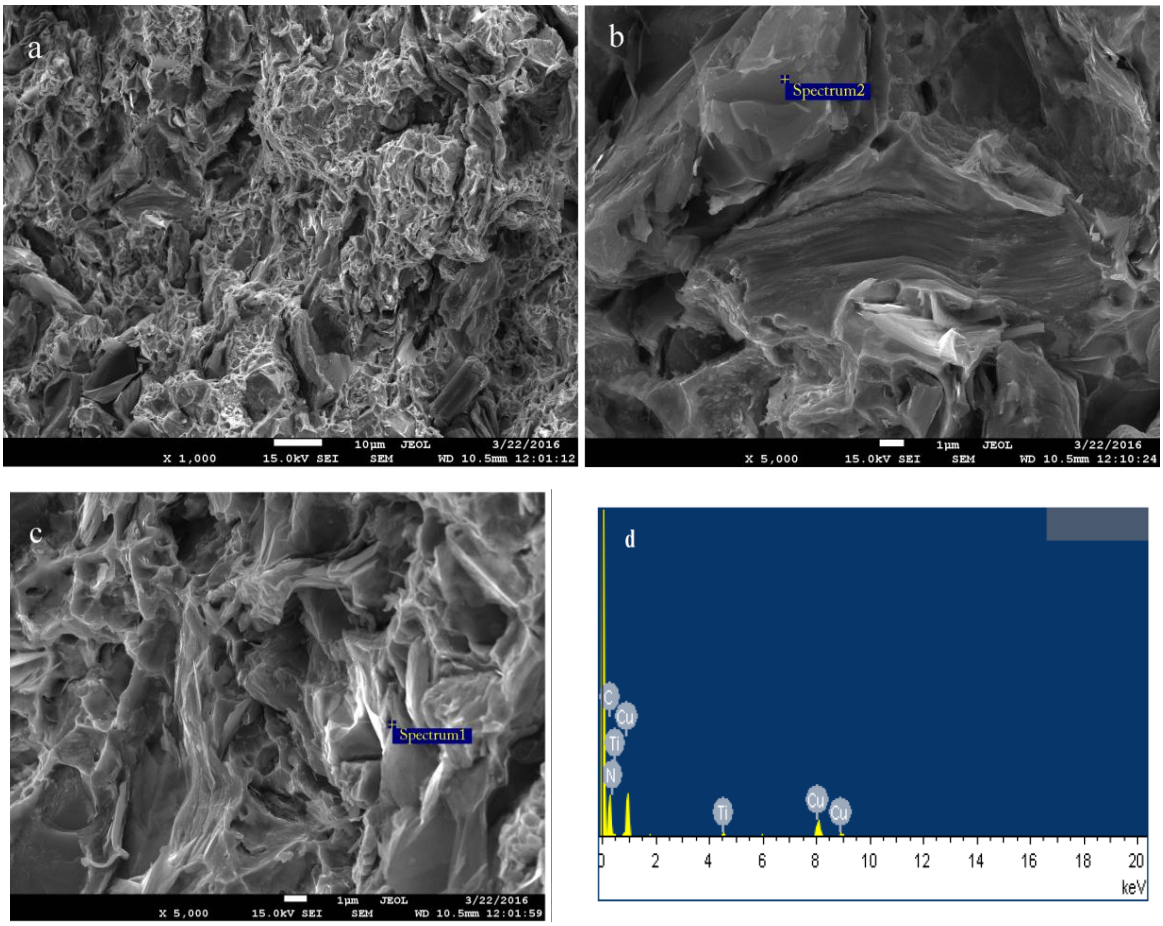

Figure 7. (**a**–**c**) SEM images of tensile fractures of the nanocomposites; (**d**) EDS element analysis of the marked lamellar spots in (**c**).

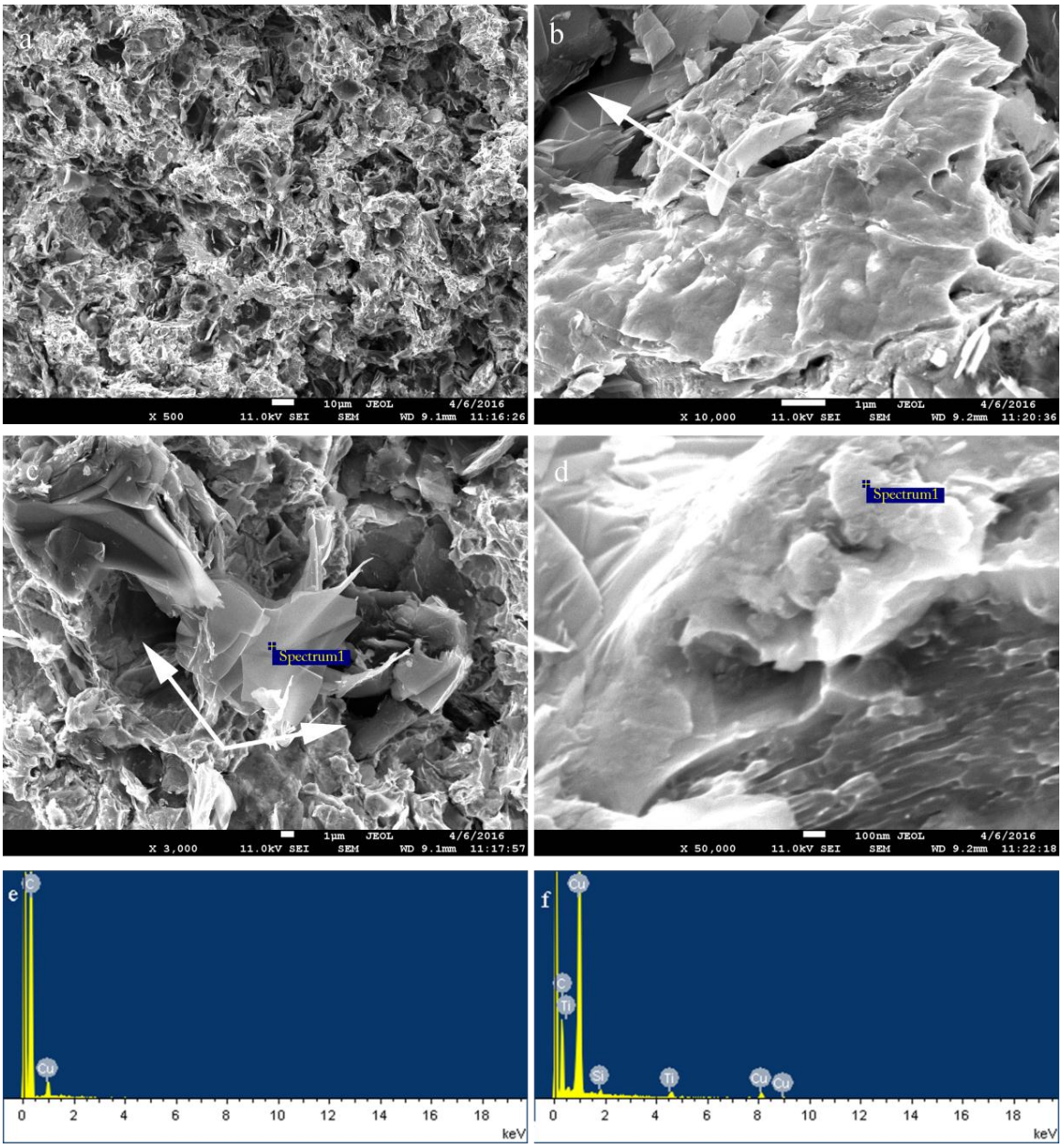

Figure 8. (**a**–**d**) SEM images of shear fractures of the nanocomposites; the EDS spectra in (**e**,**f**) are taken from the marked spots in (**c**,**d**), respectively.

3.5. Strengthening Mechanism Analysis of Cu/Ti_3SiC_2/C/BN/GNPs Nanocomposites

The possible strengthening mechanisms include second-phase strengthening, thermal mismatch and load transfer, which result from the existence of the reinforcement phases and the exclusive texture of the grapheme [13,27]. In Figure 7b, it can be observed that in the vicinity of graphite reinforcement phase, the propagation direction of shear ridges is inflected, indicating that the existence of second phase can hinder dislocation slippage to improve mechanical strength of nanocomposite materials. As shown in Figure 7c, BN is well embedded in copper matrix without pull-out, which indicates that BN and copper matrix have a good interfacial bonding strength. In addition, the thermal expansion mismatching of GNPs and Cu matrix can lead to residual stress resulting in the increase of dislocation density in matrix, which can also contribute to strengthen the nanocomposites [28]. Besides, when the interface between graphene and copper matrix combines well, it can effectively

transfer load, thus improving the strength of the composites [29]. However, the average tensile strength of nanocomposites is 168.6 MPa, which has no significant improvement compared to pure copper. It can be related to the pores existing in the nanocomposites and the poor interfacial bonding between GNPs and Cu matrix. The relative density of the Cu/Ti_3SiC_2/C/BN/GNPs nanocomposites is 98.62%, showing the existence of porosity. These voids and the poor interfacial bonding between GNPs and Cu matrix act as nucleation sites of crack initiation under external load. Cracks initiate at these locations and extend along the interfaces, resulting in the undesirable tensile and shear strength. The different effects of reinforcements on tensile and compressive strength of nanocomposite can be attributed to the different types of external loads. Under tensile load, micro-cracks are more likely to initiate at the sites of voids and interfaces, then extend along the interfaces before the external load effectively transfer from the Cu matrix to GNPs, leading to the decrease of tensile strength. However, under compressive stress, the voids are further diminished, and GNPs with better compression resistibility play a role as bearing phase, resulting in a higher compressive strength of the nanocomposites. From Figure 8c, several cavities can be observed around GNPs and copper matrix, which demonstrate that the cavities have a negative effect on the mechanical properties of nanocomposites. Henceforth, further works focusing on the enhancement of the interfacial bonding and improvement of the relative density would be carried out.

3.6. Tribological Properties and Wear Mechanisms Analysis

Orthogonality analysis had been used to study the wear behavior of Cu/Ti_3SiC_2/C/BN/GNPs composites under different working conditions. As shown in Table 2, both the average wear loss and friction coefficient of Cu/Ti_3SiC_2/C/BN/GNPs nanocomposites are much lower compared to pure copper under each separate working condition, showing a better tribological performance which could be attributed to the presence and distribution of the multi-phase reinforcements.

Table 2. Conditions and results of orthogonality analysis test.

Materials	Rotational Speed (rpm)	Load (N)	Friction Time (min)	Wear Loss (g)	Friction Coefficient
Cu/Ti_3SiC_2/C/BN/GNPs nanocomposites	50	500	15.16	0.00794	0.26175
	100	450	7.58	0.01382	0.24725
	150	400	5.05	0.01342	0.21950
	200	350	3.79	0.01283	0.22925
Copper	50	350	15.16	0.02158	0.384
	100	400	7.58	0.02712	0.349
	150	450	5.05	0.24645	0.447
	200	500	3.79	0.07638	0.38

To further understand the effects of multi-phase reinforcements on tribological behavior and the wear mechanism, worn surfaces were observed by scanning electron microscope, and the results are shown in Figure 9. The wear mechanisms might include adhesion wear, fatigue wear, wild abrasive and oxidation wear mechanisms. Figure 9a shows that the worn surface is rough but not very smeared. In Figure 9, it can be observed that the Cu matrix performed considerable plastic deformation during the friction process. The presence of Fe and Cr elements on worn surfaces (Figure 9e,f) and wear debris (Figure 10a,b) determined by EDS in Figure 10c,d, confirms that material transfer has taken place between the friction pairs, which suggests the behavior of adhesion wear. In addition, some fatigue cracks, chipping pits and a few slim abrasive furrows along the sliding direction exist on the worn surface. This suggests that fatigue and abrasive wear also occurred during the friction process. The abrasive wear is mainly attributed to the hard abrasive particles, such as TiC, Ti_3SiC_2 and oxide of matrix, which notch grooves on the surface when they are entrapped in the contact surfaces. In addition, both in worn surfaces and debris EDS patterns, a certain amount of O element is

detected, which indicates the possibility of oxidation occurred in the wear process due to the elevated temperature and oxidation wear as well.

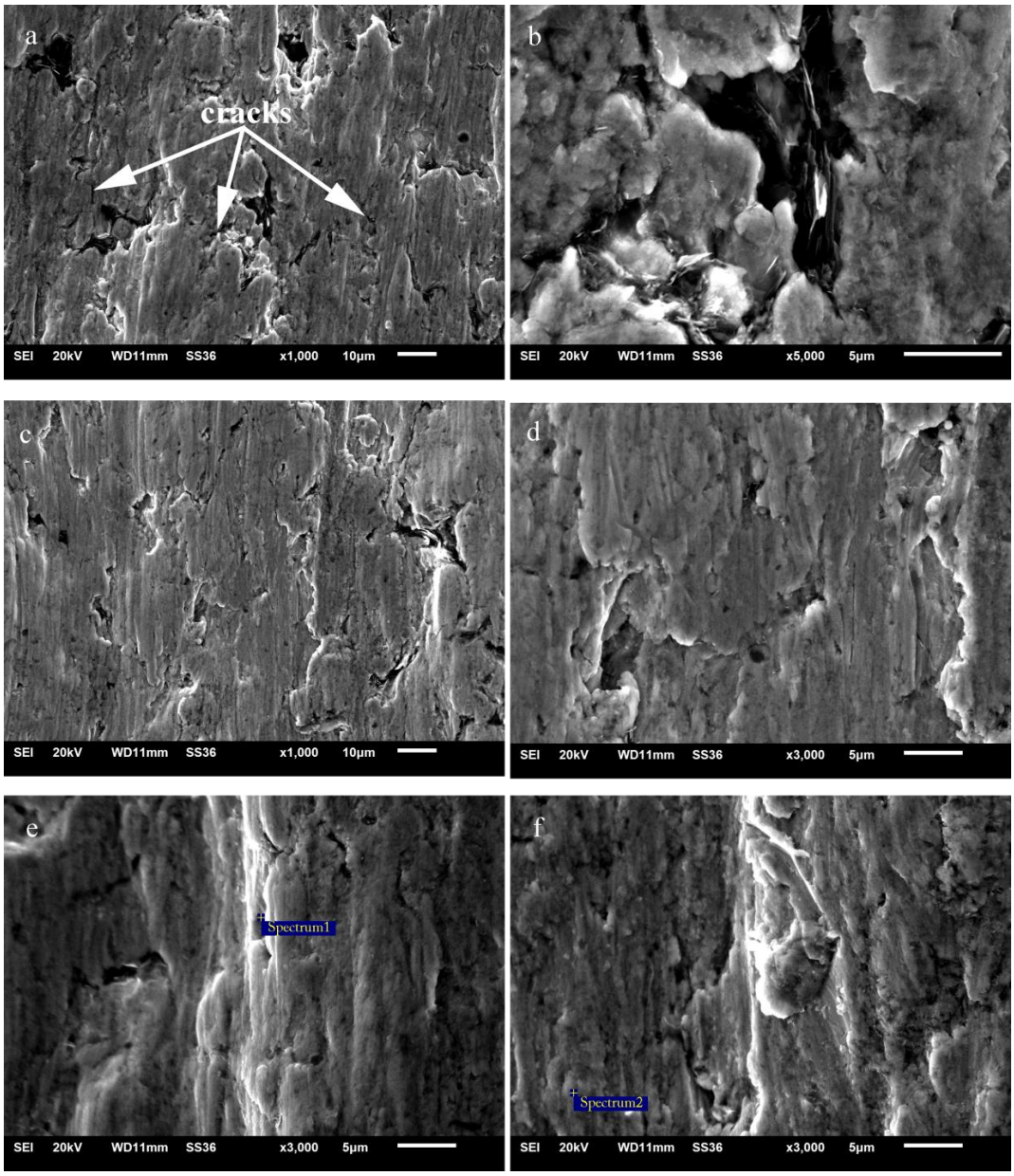

Figure 9. (**a**), (**c**), (**e**) and (**f**) SEM of worn surfaces; (**b**) and (**d**) the partial enlarged picture of (**a**) and (**c**) respectively.

Figure 10 presents the SEM images of wear debris. The wear debris are fine power-like particles or large flake-like particles with smooth surface, indicating that the dominant wear form of nanocomposites is adhesion wear [17], accompanied with fatigue, wild abrasive and oxidation wear mechanisms. From Figure 9a, sintering necks among Cu particles can be observed, meanwhile, graphite or GNPs aggregation is maintained in the holes among Cu particles, which is one of the significant reasons for the good wear resistance of nanocomposites. During the friction process, the Cu matrix deformed under the shear stress, which results in the deformation of the holes among Cu particles. Consequently, the reinforcement phases were squeezed out from the subsurface, forming a solid lubricating film on the worn surface. This reduced the direct contact area between friction pairs,

resulting in the decrease of the coefficient of friction and wear loss. The EDS results listed in Table 3 illustrate that the tribo-films consist of graphite or GNPs, BN and Ti_3SiC_2, which shows the synergistic effects of the multi-phase reinforcements. Compared with Figure 9c, the graphite or GNPs have finer structure and are more uniformly distributed in the matrix in Figure 9a. Furthermore, the worn surface is smoother and less plastic deformation has occurred. These results reveal that the finer structure and uniform distribution of graphite or GNPs contribute to more continuous and compact tribo-film, which can prevent further plastic deformation of the matrix and improve tribological properties of nanocomposites.

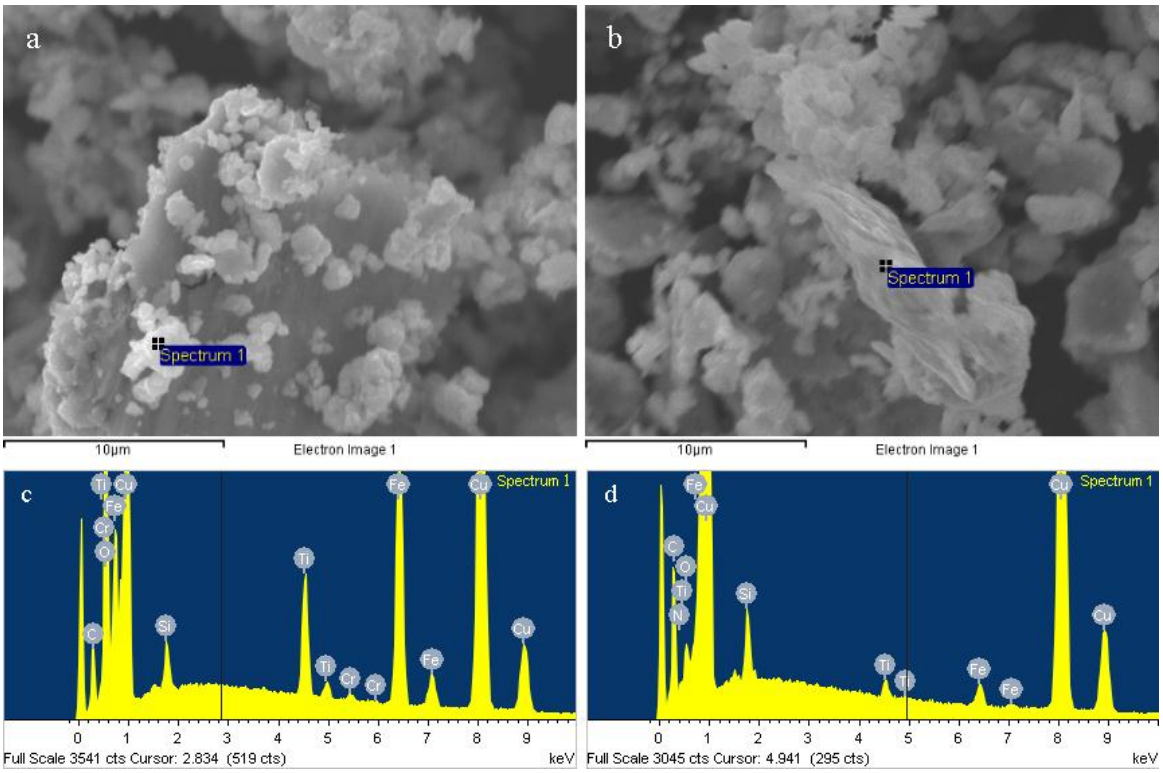

Figure 10. (**a**) and (**b**) SEM of debris surfaces; (**c**) and (**d**) the EDS spectra of the marked spot in (**a**) and (**b**), respectively.

Table 3. EDS patterns of spectra 1,2 in Figure 9e,f, respectively.

Spectrum	Element	Weight/wt. %	Atomic/at. %
1	C	24.41	62.22
	N	0.29	0.64
	Si	1.19	1.30
	Ti	0.80	0.51
	Cu	73.32	35.33
2	C	18.12	51.06
	O	2.70	5.71
	Si	1.39	1.68
	Ti	0.69	0.49
	Cu	77.09	41.06
Total		100.00	-

4. Conclusions

(1) Microstructure of Cu/Ti_3SiC_2/C/BN/GNPs nanocomposite sintered by vacuum hot-pressing and hot isostatic pressing is fine and homogeneous. The hot isostatic pressing method significantly contributes to the homogenization and densification of nanocomposites. During sintering process, TiC and Cu_9Si are generated due to thermal decomposition of Ti_3SiC_2.

(2) Ti_3SiC_2, graphite, BN and GNPs uniformly distribute in Cu matrix. There are several kinds of strengthening mechanisms of nanocomposites, including second-phase strengthening, thermal mismatch and load transfer. Different fracture mechanisms are observed in the nanocomposites, including micro-porous aggregation fractures and tears of the matrix, interfacial debonding and intergranular fractures of reinforcement phases.

(3) During the process of friction, GNPs, graphite, BN and Ti_3SiC_2 can be squeezed from the Cu matrix to form a tribo-film on the worn surface, which improves tribological properties of nanocomposites. Adhesion wear is the dominant wear form of nanocomposites accompanied with fatigue, wild abrasive and oxidation wear forms.

Acknowledgments: This work was supported by National Natural Science Foundation of China (No. 51201143), Fundamental Research Funds for the Central Universities (No. 2682015CX001), China Postdoctoral Science Foundation (No. 2015M570794), Key Laboratory of Infrared Imaging Materials and Detectors, Shanghai Institute of Technical Physics, Chinese Academy of Sciences (No. IIMDKFJJ-14-04) and Sichuan Science and Technology Support Program (No. 2016FZ0079).

Author Contributions: Zhenyi Shao and Xiaosong Jiang conducted the overall experimental design and characterization, and results analysis and discussion; Yue Sun characterized the Cu matrix nanocomposites and analyzed and discussed the results; Wanxia Liu and Xueqiao Zhang prepared the Cu matrix nanocomposites; all the authors participated in the design of the experiments and cooperated in writing this paper.

Conflicts of Interest: The authors declare no conflict of interest.

References

1. Hirotaka, K.; Masahiro, T.; Yoshiro, I.; Kazuo, W.; Yoshinori, S. Wear and mechanical properties of sintered copper-tin composites containing graphite or molybdenum disulfide. *Wear* **2003**, *255*, 573–578.
2. Gultekin, D.; Uysal, M.; Aslan, S.; Guler, M.O.; Akbulut, H. The effects of applied load on the coefficient of friction in Cu-MMC brake pad/Al-SiCp MMC brake disc system. *Wear* **2010**, *270*, 73–82. [CrossRef]
3. Jarsolav, K.; Stefan, E.; Jozef, B.; L'ubomir, K. Effect of composition on friction coefficient of Cu-graphite composites. *Wear* **2008**, *265*, 417–421.
4. Rajkumar, K.; Aravindan, S. Tribological behavior of microwave processed copper-nanographite composites. *Tribol. Int.* **2013**, *57*, 282–296. [CrossRef]
5. Dhokey, N.B.; Thool, A.D.; Spapate, S.G.; Paretkar, R.K. Influence of operating parameters on dry sliding wear of copper-based SiC composites. *J. Eng. Tribol.* **2007**, *221*, 105–114. [CrossRef]
6. Sundararajan, S.; Selwin, J.R. Investigation of microstructure, mechanical, and tribological properties of solid self-lubricating copper hybrid composites processed by solid-state mixing technique. *Eng. Tribol.* **2016**, *230*, 40–56. [CrossRef]
7. Zhao, H.J.; Liu, L.; Wu, Y.T.; Hu, W.B. Investigation on wear and corrosion behavior of Cu-graphite composites prepared by electroforming. *Compos. Sci. Technol.* **2007**, *67*, 1210–1217. [CrossRef]
8. Moustafa, S.F.; El-Badry, S.A.; Sanad, A.M.; Kieback, B. Friction and wear of copper-graphite composites made with Cu-coated and uncoated graphite powders. *Wear* **2002**, *253*, 699–710. [CrossRef]
9. Li, J.F.; Zhang, L.; Xiao, J.K.; Zhou, K.C. Sliding wear behavior of copper-based composites reinforced with graphene nanosheets and graphite. *Trans. Nonferr. Met. Soc. China* **2015**, *25*, 3354–3362. [CrossRef]
10. Chen, S.Y.; Li, X.R.; An, D.; Liang, J.; Liu, C.S. Preparation and wear performance of novel graphite/copper alloy-matrix self-lubricating composite materials. *Adv. Mater. Res.* **2014**, *941*, 284–287. [CrossRef]
11. Larionova, T.; Koltsova, T.; Fadin, Y.; Tolochko, O. Friction and wear of copper-carbon nanofibers compact composites prepared by chemical vapor deposition. *Wear* **2014**, *319*, 118–122. [CrossRef]

12. Afsaneh, D.M.; Emad, O.; Pradeep, L.M.; Pradeep, K.R. Mechanical and tribological properties of self-lubricating metal nanocomposites reinforced by carbon nanotubes (CNTs) and grapheme—A review. *Compos. Part B* **2015**, *77*, 402–420.
13. Zhang, D.D.; Zhan, Z.J. Preparation of graphene nanoplatelets-copper composites by a modified semi-powder method and their mechanical properties. *J. Alloy. Compd.* **2016**, *658*, 663–671. [CrossRef]
14. Cao, T.K.; Xiao, Z.J. Tribological Behaviors of Self-lubricating Coating Prepared by Electrospark Deposition. *Tribol. Lett.* **2012**, *56*, 231–237. [CrossRef]
15. Chen, S.Y.; Bi, Y.N.; Zhang, H.L.; Liang, J.; Wellburn, D.; Liu, C.S. Effect of BN fraction on the mechanical and tribological properties of Cu alloy/BN self-lubricating sleeves. *J. Compos. Mater.* **2015**, *49*, 3715–3725. [CrossRef]
16. Omayma, A.M.; Ahmed, A.O.; Emad, M.M.; Sheikh, M.E. Physico-mechanical and tribological properties of Cu/h-BN nanocomposites synthesized by PM route. *J. Alloy. Compd.* **2015**, *625*, 309–317.
17. Chen, B.M.; Bi, Q.L.; Yang, J.; Xia, Y.Q.; Hao, J.C. Tribological properties of solid lubricants (graphite, h-BN) for Cu-based P/M friction composites. *Trib. Int.* **2008**, *41*, 1145–1152. [CrossRef]
18. Zhou, Y.; Chen, B.; Wang, X.; Yan, C. Mechanical properties of Ti_3SiC_2 particulate reinforced copper prepared by hot pressing of copper coated Ti_3SiC_2 and copper powder. *Mater. Sci. Technol.* **2004**, *20*, 661–665. [CrossRef]
19. Chu, K.; Jia, C. Enhanced strength in bulk Graphene-copper composites. *Phys. Status Solidi A* **2014**, *211*, 184–190. [CrossRef]
20. Jiang, X.S.; Liu, W.X.; Li, J.R.; Shao, Z.Y.; Zhu, D.G. Microstructures and mechanical properties of $Cu/Ti_3SiC_2/C$/MWCNTscomposites prepared by vacuum hot-pressing sintering. *J. Alloy. Compd.* **2015**, *618*, 700–706.
21. Lu, Q.; He, G.Q.; Yang, Y.; Fan, K.L.; Zhao, X.G. Friction and Wear Property of a New Cu-based $Cu/Ti_3SiC_2/C$ composite. *Chin. J. Mater. Res.* **2015**, *29*, 216–220.
22. Geim, A.K.; Novoselov, K.S. The Rise of Graphene. *Nat. Mater.* **2007**, *6*, 183–191. [CrossRef] [PubMed]
23. Zhang, Y.; Zhou, Y.C. Ti_3SiC_2 dispersion-strengthened copper: A new dispersion-strengthened copper alloy. *Acta Metall. Sin.* **2000**, *36*, 662–666.
24. Gorny, G.; Raczka, M.; Stobierski, L.; Rozniatowski, K.; Rutkowski, P. Ceramic composite Ti_3SiC_2-TiB_2-Microstructure and mechanical properties. *Mater. Charact.* **2009**, *60*, 1168–1174. [CrossRef]
25. Zhang, J.D.; Li, C.J.; Zhu, X.K.; Li, G. Effect of Severe Plastic Deformation (SPD) on the Mechanical Properties of Pure Cu. *Yunnan Metall.* **2007**, *36*, 56–68.
26. Larionova, T. Copper-based Composite Materials Reinforced with Carbon Nanostructures. *Mater. Sci.* **2015**, *21*, 364–368. [CrossRef]
27. Youbin, K.; Jinsup, L.; Min, S.Y. Strengthening effect of single-atomic-layer graphene in metal-graphene nanolayered composites. *Nat. Commun.* **2013**, *4*, 1–7.
28. Kim, W.J.; Lee, T.J.; Han, S.H. Multi-layer graphene/copper composites: Preparation using high-ratio differential speed rolling, microstructure and mechanical properties. *Carbon* **2014**, *69*, 55–65. [CrossRef]
29. Prashantha, H.G.; Anthony, X.M. Graphene Reinforced Metal Matrix Composite (GRMMC): A Review. *Procedia Eng.* **2014**, *97*, 1033–1040.